

pubs.acs.org/JPCL Letter

# Excited-State-Selective Ultrafast Relaxation Dynamics and Photoisomerization of *trans-4,4'*-Azopyridine

Laura M. Obloy, Patrick Z. El-Khoury,\* and Alexander N. Tarnovsky\*



Cite This: J. Phys. Chem. Lett. 2022, 13, 10863-10870



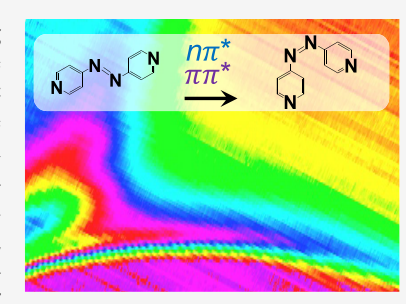
**ACCESS** I

III Metrics & More

Article Recommendations

Supporting Information

**ABSTRACT:** Excited-state dynamics of *trans*-4,4'-azopyridine in ethanol is studied using femtosecond transient absorption with 30 fs temporal resolution. Exciting the system at three different wavelengths, 460 and 290 (275) nm, to access the  $S_1$   $n\pi^*$  and  $S_2$   $\pi\pi^*$  electronic states, respectively, reveals a 195 cm<sup>-1</sup> vibrational coherence, which suggests that the same mode is active in both  $n\pi^*$  and  $\pi\pi^*$  relaxation channels. Following  $S_1$ -excitation, relaxation proceeds via a nonrotational pathway, where a fraction of the  $n\pi^*$  population is trapped in a planar minimum (lifetime, 2.1 ps), while the remaining population travels further to a second shallow minimum (lifetime, 300 fs) prior to decay into the ground state. Population of the  $S_2$  state leads to 30 fs nonrotational relaxation with a concurrent buildup of  $n\pi^*$  population and nearly simultaneous formation of hot ground-state species. An increase in the *cis*-isomer quantum yield upon  $\pi\pi^*$  versus  $n\pi^*$  excitation is observed, which is opposite to *trans*-azobenzene.



The unique photochromic properties of azobenzene derivatives have stimulated a great amount of fundamental and applied research. 1-3 These photochromic systems can be reversibly switched between their trans and cis isomeric forms by exposure to light that is resonant with their dipoleforbidden  $S_1$   $n\pi^*$  and dipole-allowed  $S_2$   $\pi\pi^*$  states. 1,4,5 Photoisomerization in azobenzene derivatives was generally discussed in terms of rotational and nonrotational mechanisms involving twisting around the N=N double bond and in-plane inversion at one of the two N atoms.6 The most prominent representative of these photoswitches, trans-azobenzene (TAB), has been extensively studied by a variety of timeresolved spectroscopic techniques 7-17 and tools of computational quantum chemistry. 6,18-28 When  $S_1$   $n\pi^*$  and  $S_2$   $\pi\pi^*$ states are selectively excited in TAB, the quantum yield of photoisomerization is halved from 0.20-0.35 (S<sub>1</sub>) to 0.05-0.15 (S<sub>2</sub>) depending on solvent viscosity and polarity.<sup>29,30</sup> This intriguing excited-state dependence of the photoisomerization quantum yield is thought to be due to the predominance of the rotational pathway in  $S_1 n\pi^*$  and the nonrotational pathway in  $S_2 \pi \pi^*$ . That said, unambiguous assignment and/or separation of these reaction pathways has been challenging, and mixed reaction mechanisms 1,6-8,30,18,27,30 and intermediate excited electronic states 15,16,19 have been proposed. According to a recent theoretical analysis,<sup>6</sup> the  $S_1$   $n\pi^*$  excitation favors a rotational pathway, which proceeds through a conical intersection (CI<sub>1</sub>) leading to the ground-state (GS)  $S_0$ minimum of either the cis- or trans-isomer (Figure 1a). A second intersection (CI<sub>2</sub>) on the pedal-like reaction pathway separates the cis and trans minima; however, this pathway and CI2 are energetically disfavored from the Franck-Condon (FC) region. Femtosecond fluorescence anisotropy measure-

ments<sup>9</sup> and high-resolution scanning of the S<sub>1</sub> and S<sub>2</sub> potential energy surfaces (PESs) by multiphoton ionization<sup>14</sup> both support the hypothesis of a rotational mechanism on  $S_1$   $n\pi^*$ , although some ultrafast transient absorption studies suggest a more complex picture that involves biphasic decay of this state. 11,12 Theoretical analyses further suggest that in the S2  $\pi\pi^*$  state a pedal-like, barrierless pathway leads to a  $\pi\pi^*/n\pi^*$  $CI_3$  and then proceeds analogously to  $n\pi^*$  excitation to the rotated  $n\pi^*/S_0$  CI<sub>1</sub>. A less prominent rotational pathway via a  $\pi\pi^*/n^2\pi^{*2}$  CI<sub>4</sub> could explain the lower photoisomerization quantum yields upon  $\pi\pi^*$  excitation. Experimental work<sup>13</sup> found that half of the initial  $\pi\pi^*$  population relaxes to an S<sub>1</sub> region not accessible upon  $n\pi^*$  excitation, where a substantial part reaches the trans GS. Recent transient absorption spectroscopy experiments with 20 fs temporal resolution were able to resolve a single  $\sim$ 50 fs lifetime of the  $\pi\pi^*$  state with a concurrent buildup of hot  $n\pi^*$  population.<sup>17</sup> It was proposed that hot  $n\pi^*$  population proceeds through an energetically high-lying near-planar region of the  $n\pi^*/S_0$  CI seam, which is inaccessible upon  $n\pi^*$  excitation and has a preference for *trans* over *cis* S<sub>0</sub> formation. The coherent motion observed in the 195 cm<sup>-1</sup> CNN in-plane bending mode marked the presence of this nonreactive channel, which

Received: August 14, 2022 Accepted: October 20, 2022 Published: November 16, 2022





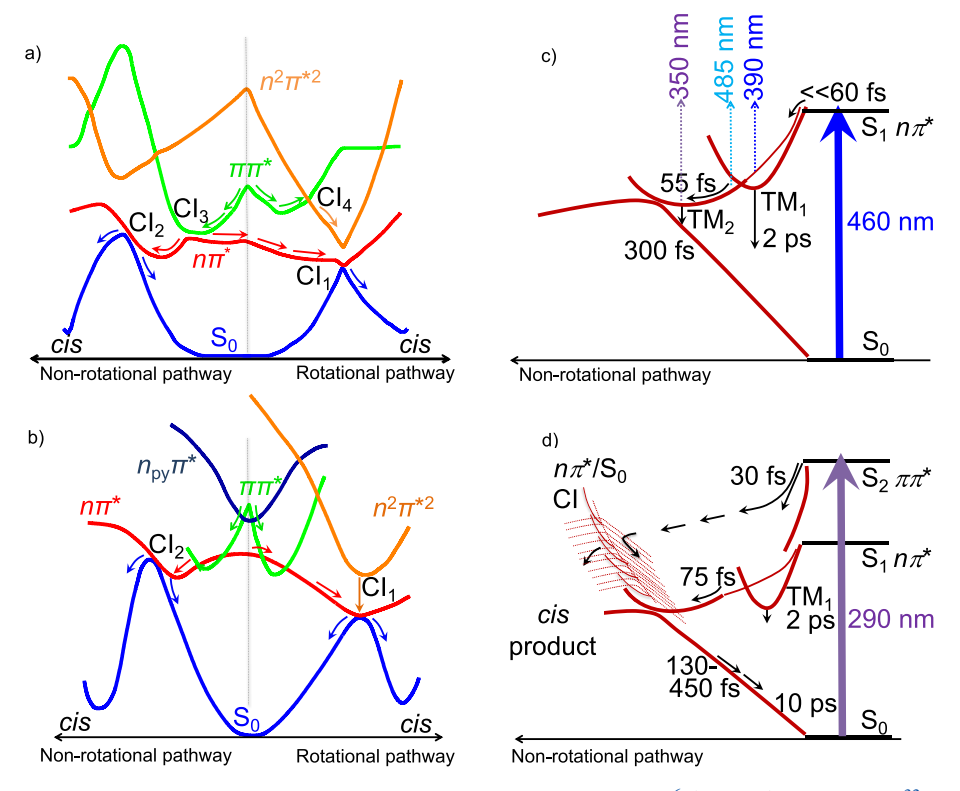


**Figure 1.** Photoisomerization path of TAB in  $S_1$   $n\pi^*$  and  $S_2$   $\pi\pi^*$  states, and the involved CIs<sup>6</sup> (a and b). For 3-PAPy,  $^{32}$   $\pi\pi^*$  and  $n\pi^*$  states mix, causing a local planar and a global rotated minima on the  $n\pi^*$  surface, and the planar  $n\pi^*/S_0$  CI (CI<sub>2</sub>) is 6 kcal/mol (8 kcal/mol in 4-PAPy<sup>34</sup>) above the FC point (defined in panels a and b by thin vertical lines). A summary of this work on 4,4'-APy (c and d). The 460 nm  $S_1$   $n\pi^*$  FC region is depopulated within 60 fs (c). The  $n\pi^*$  population that is not trapped in the planar TM<sub>1</sub> minimum descends toward a shallow TM<sub>2</sub> minimum reached in ~55 fs, where it decays with a 300 fs lifetime into  $S_0$ . The 290 nm  $S_2$   $\pi\pi^*$  population decays with a 30 fs lifetime into the  $n\pi^*$  state, where one fraction relaxes likewise upon  $n\pi^*$  excitation (d). The remaining population reaches a high-energy region of the planar  $n\pi^*/S_0$  CI seam, and branches into either hot *cis*- or *trans*- $S_0$  forms that undergo vibrational relaxation over ~0.13–10 ps time scales.

accounts for the reduced photoisomerization quantum yield upon  $\pi\pi^*$  excitation.<sup>17</sup>

Substituted azopyridines are interesting and promising photoresponsive compounds  $^{31-34}$  The nitrogen atom of pyridine introduces a lone pair of  $n_{py}$  electrons, where one can be promoted to the azo  $\pi^*$  molecular orbital introducing new excited states of  $n_{pv}\pi^*$  nature, which can alter the relaxation pathway. Computational studies of trans-3-phenylazopyridine (3-PAPy),<sup>32</sup> and trans-4-phenyl-azopyridine (4-PAPy),<sup>34</sup> which are closely related to trans-4,4'-azopyridine (4,4'-APy) studied in this work, suggest a complex  $S_1$   $n\pi^*$ topology with a local near-planar minimum and a global rotated minimum, which in 3-PAPy is caused by mixing with a close-lying  $S_2$   $\pi\pi^*$  surface<sup>32</sup> (Figure 1b). The dominant rotational pathway eventually leads to a rotated  $n\pi^*/S_0$  CI, where branching occurs into either the cis or trans forms. If 3-PAPy is excited into the  $S_2 \pi \pi^*$  state, rotational relaxation from the FC region is predicted.<sup>32</sup> Experimental work on the excited-state dynamics and photoisomerization pathways of azopyridines is very limited. By studying 4,4'-APy we strive to answer several questions, including (i) whether the excited states exhibit similar behavior to what is known from structurally related azobenzene systems and (ii) whether the topologies of the PES involved are unique. This should lead to a deeper understanding of photochromism in azo compounds in general.

The spectral position and relative strength of the UV-vis absorption bands of 4,4'-APy (Sigma-Aldrich) are similar to those of TAB (325 and 450 nm<sup>10</sup>) and other phenyl

azopyridines in ethanol (Figure 1SI; 317 and 456 nm for 3-PAPy,<sup>32,35</sup> 312 and 454 nm for 4-PAPy<sup>35</sup>) and can be similarly assigned to transitions into the S<sub>2</sub>  $\pi\pi^*$  and S<sub>1</sub>  $n\pi^*$  states (Figure 2a). Note that the 285 nm band of 4,4'-APy is broader by ~2000 cm<sup>-1</sup> compared to the  $\pi\pi^*$  transition of TAB and the UV bands of 3- and 4-PAPy, which may be indicative of another electronic transition that contributes to the 285 nm band in addition to the  $\pi\pi^*$  transition (Figure 1SI). Under continuous 365 nm irradiation, the formation of a product band and bleaching of 4,4'-APy absorption is observed (Figure 3SI). The shape of the difference absorption spectrum (Figure 2d) and the absorption recovery, which occurs with a time constant of 18.9 min in the dark, are analogous to the spectral appearance and kinetic stability of cis-isomers of azobenzenes,<sup>5</sup> and therefore, the observations are attributed to trans-cis isomerization of 4,4'-APy. Irradiation for 2 min with a 1 kHz train of 460 nm pulses yielded a factor of 1.8 smaller photoisomerization quantum yield compared to 290 nm pulses (Figure 4SI).

Upon 460 nm 40 fs excitation of a flowing ethanol jet with 4,4'-APy, the  $\Delta A$  signals in the 340–650 nm probing region exhibit a pulse-limited rise with the formation of the 387 nm band with a broad 475–525 nm shoulder (Figure 2b). The very initial dynamics likely involve the earliest excited-state species, and consequently, the 0 fs  $\Delta A$  spectrum can be assigned to excited-state absorption (ESA) of 4,4'-APy molecules from the planar FC region of the S<sub>1</sub>  $n\pi^*$  state. As the excitation pulse continues to populate this region to 30 fs, the 387 nm  $\Delta A$  band grows, but the shoulder does not. This is

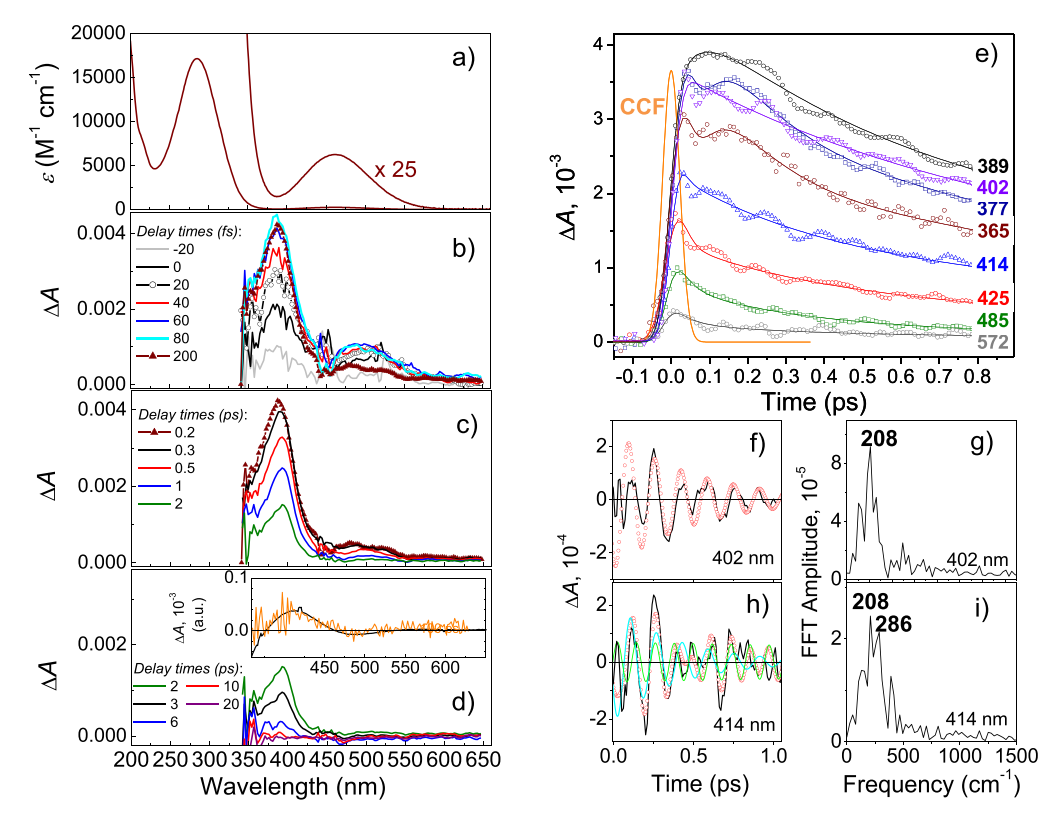


**Figure 2.** 285 and 464 nm absorption bands of 4,4'-APy in ethanol with the molecular decadic extinction coefficient ( $\varepsilon$ ) of 17,148 and 254 M<sup>-1</sup> cm<sup>-1</sup> (a). Short (b), intermediate (c), and long (d) time Δ*A* spectra of 4,4'-APy. Delay times between the 460 nm excitation and probe pulses are given in the legends. The 1 ns Δ*A* spectrum (orange, inset in panel d), agrees with the amplitude-scaled *trans–cis* difference absorption spectrum (black) from continuous irradiation experiments. Multiexponential fits (lines) of sub-1 ps Δ*A* kinetic traces from 365 to 572 nm (symbols) are obtained by deconvolution with the pump–probe CCF (50 fs fwhm, Gaussian-shaped) (e). The 402 and 414 nm residuals (black lines) of such fits are fitted using exponentially damped cosine functions (red symbols) (f and h); 195 cm<sup>-1</sup> modulations at 402 nm and 201 (cyan) and 278 cm<sup>-1</sup> (green) modulations at 414 nm are found. FFT analysis of the residuals is given in panels g and i.

evidence that the earliest species relax into another species (denoted as  $TM_1$ ), which absorb at ~390 nm but less around 475-525 nm (Figure 1c). Since this relaxation happens within the first 30 fs, it is thought not to involve a large-amplitude deformational motion, which requires longer time scales. This suggests that the TM<sub>1</sub> species have a nearly planar geometry. From 50 to 150 fs,  $\Delta A$  signals decay in the red (~35 fs time constants, Table 1SI) while developing slower between 340 and 420 nm (a 40-70 fs wavelength-dependent rise), which constitutes a blue shift of a broad transient absorption overlaid with the 390 nm band. This evolution ends with a decay of a single 300 fs time constant. The 100-150 fs hump in the 350-425 nm  $\Delta A$  kinetic traces (Figure 2e) is due to superposition of the 65 fs rise and 300 fs decay processes; the spectral profiles of these two components resemble each other (Figure 11SI), suggesting their common origin. When molecules descend along the barrierless surface to a lower portion of the PES, the molecular absorption from the initial region decays whereas that from the lower portion rises; the rise time constant becomes longer when probing lower-energy distant portions of the potential.<sup>36</sup> Therefore, the  $\sim$ 35–70 fs blue shift is evidence that a fraction of the population relaxes along the  $n\pi^*$  potential toward its lower portion. There, the exit channel into the GS is located; its 300 fs lifetime suggests that it is best described as a very shallow trap minimum (TM<sub>2</sub>). This decay ultimately unmasks the 393 nm  $\Delta A$  band (with a weak 485 nm shoulder) of the TM<sub>1</sub> species. Their absorption decays singleexponentially with a 2.1 ps lifetime, suggesting that TM<sub>1</sub>

corresponds to a more pronounced minimum on the  $n\pi^*$  PES. As  $TM_1$  stores a 460 nm photon energy as electronic excitation, these species carry little vibrational excitation, consistent with minor narrowing of their 393 nm  $\Delta A$  band with time.

Subpicosecond  $\Delta A$  kinetic traces display damped coherent modulations (Figure 2e). The oscillatory residuals  $R(\lambda, t)$  were obtained by subtracting multiexponential fits that use deconvolution with a cross-correlation-function (CCF) from the respective  $\Delta A$  kinetic traces. Fast Fourier transform (FFT) analysis of  $R(\lambda, t)$  signals reveals the presence of two different frequencies at  $\sim$ 195 and  $\sim$ 270 cm<sup>-1</sup> (Figures 2f-i and 12SI). Their observed frequency varies within 182-208 and 254-290 cm<sup>-1</sup> ranges (Table 2SI), reflecting the experimental and analysis accuracy. The  $R(\lambda, t)$  residuals were fitted to a sum of two exponentially damped cosine functions; the thus derived frequencies agree with those obtained by FFT (Figure 13SI and Table 3SI). Impulsive stimulated Raman scattering (ISRS) oscillations<sup>37</sup> occur via excitation of fundamental vibrational modes of the parent whose frequencies fall within the excitation pulse bandwidth: 366 cm<sup>-1</sup> (fwhm) for a transform-limited, Gaussian 40 fs pulse. A brief initial sub-10 fs passage of the wavepacket on the excited PES is sufficient for generating enough displacement for ISRS to induce the vibrational wavepacket on the GS surface.<sup>38</sup> The 270 cm<sup>-1</sup> oscillations start at negative delay times as soon as excitation and probe pulses begin to temporally overlap (Figure 14SI) and can therefore be assigned to impulsively excited vibrational

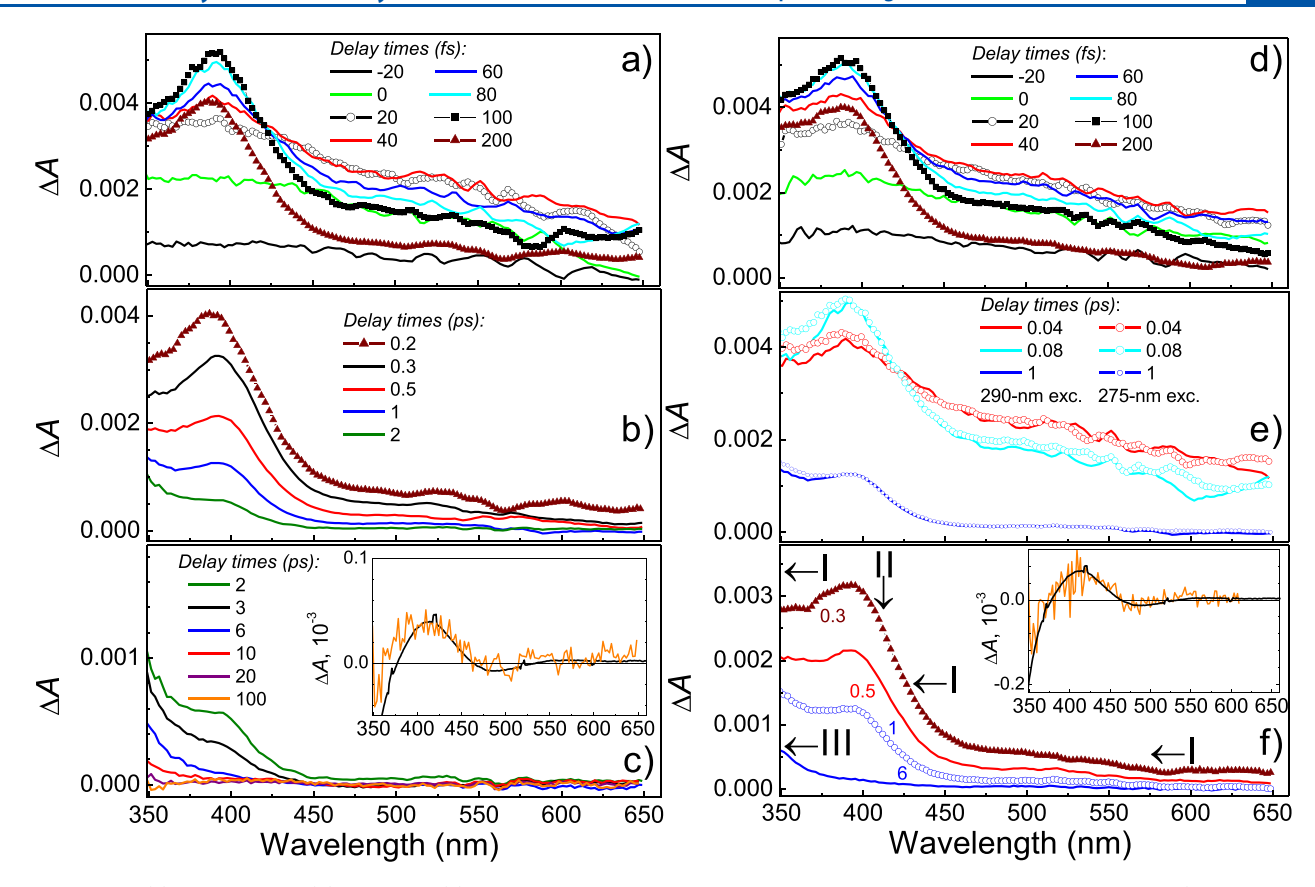


Figure 3. Short (a), intermediate (b), and long (c) time  $\Delta A$  spectra of 290 nm excited 4,4′-APy, and the 100 ps  $\Delta A$  spectrum (inset in panel c, orange) with the scaled trans-cis difference absorption spectrum (black). Following 275 nm excitation (d-f), sub-200 fs  $\Delta A$  spectra show the amplitude difference (the 345–370 nm range) compared to the 290 nm  $\Delta A$  spectra starting at 40 fs (d and e). The 0.3, 0.5, 1, and 6 ps  $\Delta A$  spectra in panel f illustrate three major processes after the initial 100 fs: the blue shift on multiple time scales (~100–900 fs time constants) due to hot S<sub>0</sub> species (I), the 2.1 ps  $n\pi^*$  TM<sub>1</sub> 390 nm band decay (II), and the several picosecond blue shift (III) due to vibrational relaxation in the S<sub>0</sub> bottom. The inset in panel f shows the 1000 ps  $\Delta A$  spectrum (orange) with the scaled trans-cis difference absorption spectrum (black).

coherence in the GS. On the other hand, when the 195 cm<sup>-1</sup> oscillations are extrapolated to delay times shorter than 50 fs, they beat asynchronously with the  $R(\lambda, t)$  residuals; such a behavior suggests vibrational coherence in a nascent product state.<sup>39-41</sup>

Small transient absorption remaining after 6 ps is due to vibrationally hot  $S_0$  species. These 350–415 nm  $\Delta A$  signals blue shift and decay on a several ps time scale, which is typical to vibrational relaxation of neutral polyatomic solutes. The decay lengthens at shorter probe wavelengths (8 ps for 350–370 nm, Table 1SI), the established wavelength dependence of vibrational relaxation in which the population situated closer to the well bottom, where the potential is nearly harmonic and the density of states is not large, relaxes with a longer time constant. A  $\Delta A$  signal that remains after completion of vibrational relaxation (20 ps) is constant in amplitude up to the longest investigated 1 ns delay time; its spectral shape agrees with the *trans-cis* difference absorption spectrum from continuous irradiation experiments (Figure 2d, inset).

The  $\Delta A$  dynamics upon excitation of 4,4'-APy at wavelengths longer (290 nm) or shorter (275 nm) than the 285 nm band maximum are very similar, suggesting similar excited-state relaxation mechanisms (Figures 15SI and 16SI. As the 290 nm excitation pulse populates S<sub>2</sub>, ESA from this  $\pi\pi^*$  state emerges (0 fs  $\Delta A$  spectrum, Figure 3a), which is seen as broad and structureless transient absorption between 350 and 650 nm. The decay of this ESA leads to the 390 nm  $\Delta A$  band, which

shapes at 60 fs, and the onset of which is observed as early as 40 fs following both 290 and 275 nm excitation (Figures 3a,d, 17SI, and 18SI). This band (decay time constant,  $2.1 \pm 0.5$  ps, Tables 4SI and 5SI) is analogous to the distinct 390 nm  $\Delta A$  band observed following 460 nm excitation (Figure 19SI) and, therefore, can be assigned to the population trapped in the  $n\pi^*$  TM<sub>1</sub> minimum. The fits yield a ~30 fs time constant for decay of the initial  $n\pi^*$  S<sub>2</sub> ESA and rise of the  $n\pi^*$  S<sub>1</sub> ESA (Tables 4SI and 5SI). Figure 3 shows that from 60 to 120 fs the  $\Delta A$  signals from ~450 to 650 nm continue to decay, whereas the  $\Delta A$  signals at shorter wavelengths (345–450 nm) rise, which resembles the blue shift observed for 460 nm excitation.

Analogous to 460 nm excitation, oscillations at ~270 cm<sup>-1</sup> induced by ISRS and other oscillations with a ~195 cm<sup>-1</sup> frequency are observed in the short-time  $\Delta A$  kinetic traces (Figures 4a–e and 20SI–24SI). The ~195 cm<sup>-1</sup> oscillations clearly occur out of phase at the blue and red wings of the 390 nm  $\Delta A$  band (the  $\pi$ -phase shift, Figure 22SI). This behavior suggests coherent vibrational motion taking place on the PES being probed, <sup>39–41</sup> and therefore, the 195 cm<sup>-1</sup> oscillations can be assigned to vibrational coherence in the TM<sub>1</sub> potential well. The wavepacket emerges on the  $n\pi^*$  surface rapidly; an onset of the 195 cm<sup>-1</sup> oscillations (~40 fs, 290 nm excitation) is consistent with  $S_2$   $\pi\pi^* \rightarrow S_1$   $n\pi^*$  internal conversion in just 30 fs. The 195 cm<sup>-1</sup> mode can be assigned to symmetric in-plane bending in the central CNNC fragment; computations yielded a 205 cm<sup>-1</sup> frequency of the CNN-bending mode at the  $n\pi^*$ 

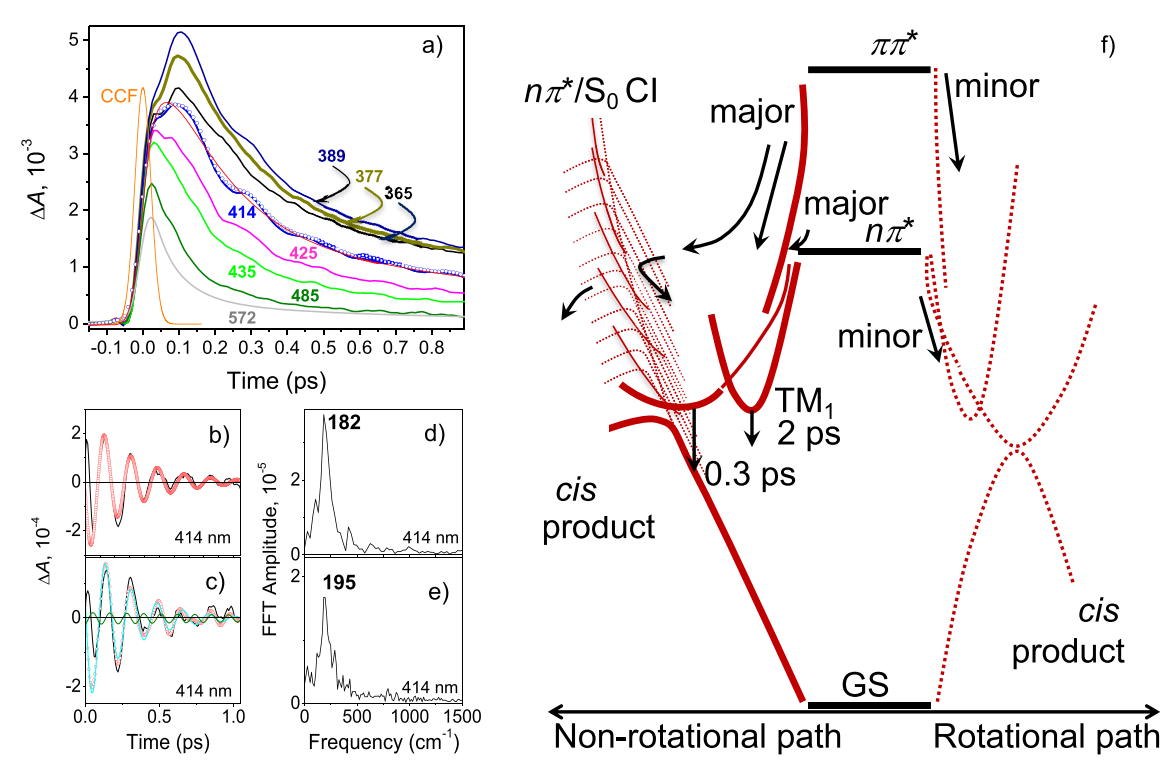


Figure 4. 290 nm excitation: the 50 fs CCF (orange) and sub-1 ps  $\Delta A$  kinetic traces (lines) (a). The 414 nm  $\Delta A$  trace with its fit (red curve) and the same trace following 275 nm excitation (symbols) illustrate the similarity between the 290 and 275 nm induced dynamics (see also Figures 15SI and 16SI). Excitation at 290 and 275 nm pertain to panels (b,d) and (c,e), respectively. The 414 nm fit residuals (black line) fitted with exponentially damped cosine functions (red symbols) reveal either ~195 cm<sup>-1</sup> modulation (b) or modulations at ~270 (green) and ~195 cm<sup>-1</sup> (cyan) (c). FFT analysis of these residuals is given in panels d and e. Both  $\pi\pi^*$  and  $\pi\pi^*$  excitations lead to the substantial population of TM<sub>1</sub>; the  $\pi\pi^*$  population decays with a 30 fs lifetime with the concurrent TM<sub>1</sub> buildup and a somewhat slower hot S<sub>0</sub> buildup, and the *cis*-isomer product yield is larger upon  $\pi\pi^*$  excitation, as summarized in panel f. The rotational topology<sup>32</sup> is not addressed here because the results suggest that this pathway is minor for 4,4′-APy.

minimum of TAB.<sup>17</sup> The decoherence time constants of the 195 cm<sup>-1</sup> oscillations become shorter upon 290 and 275 nm excitation (0.29  $\pm$  0.07 and 0.34  $\pm$  0.11 ps, respectively) compared with 460 nm excitation (0.43  $\pm$  0.05; Table 3SI), which is consistent with a faster dephasing as the density of states and anharmonicity increase with excess vibrational energy.<sup>37,44</sup> This also explains why vibrational coherence induced by ISRS in the GS well bottom dissipates much slower (several picoseconds for 270 cm<sup>-1</sup> oscillations; Table 3SI).

Spectral evolution after the initial 100 fs is illustrated in Figure 3f. As seen from the  $\Delta A$  spectra accounted for the 2.1 ps decay of the 390 nm band (Figure 25SI), absorption of hot GS species reaches the red wavelengths at short delay times. The decay of this absorption is wavelength-dependent with time constants ranging from fast to intermediate and slower: from ~100 to 900 fs and then (between 340 and 370 nm) to 4-8 ps (Tables 4SI and 5SI), reflecting vibrational relaxation in the upper, middle, and bottom parts of the GS potential, respectively. There are two minor contributions to this process, namely, the TM<sub>2</sub> population decay and the TM<sub>1</sub> vibrational relaxation. The population lifetime can be determined from the time evolution of the associated spectrally integrated  $\Delta A$ band<sup>45</sup> under the assumption that the transition dipole moment is conserved. Exponential fits of the  $\Delta A$  signals spectrally integrated from 340 to 370 nm, where the TM<sub>2</sub> species absorb according to the previous (460 nm excitation) assignment, yield the same  $0.31 \pm 0.07$  ps time constant. Further, by comparing the narrowing of the 390 nm  $\Delta A$  band

with time for 290 nm vs 460 nm, we noted that the  ${\rm TM_1}$  population undergoes vibrational relaxation on a 0.5–1 ps time scale.

All  $\Delta A$  spectra following 275 and 290 nm excitation are superimposable apart from the 345-370 nm region, where the 275 nm-induced signals are more intense. This  $\Delta A$  amplitude difference develops at 40 fs following the decay of the FC S2  $\pi\pi^*$  state and the population buildup in the S<sub>1</sub>  $n\pi^*$  state but is not related to the  $TM_1$  390 nm  $\Delta A$  band for which the maximum and red-wing signals do not change appreciably. The 345-370 nm  $\Delta A$  amplitude difference persists until ~10 ps, a time scale coinciding with that of vibrational relaxation in the S<sub>0</sub> bottom (Figures 17SI and 18SI). In one interpretation, a 40 fs time lag can be viewed as a delayed arrival of the 275 nm versus the 290 nm induced population into the same GS region monitored at 345-370 nm. That said, there is no effect on the TM<sub>1</sub> population. Alternatively, upon 275 nm excitation, a fraction of 4,4'-APy molecules is excited into the pyridinelocalized  $\pi\pi^*$  state and then decays into the GS via the pyridine-localized  $n\pi^*$  state, thereby bypassing the azo  $n\pi^*$ state altogether. These pyridine-localized states were not previously considered in the contexts of excited-state relaxation.<sup>32</sup> For isolated pyridine, the  $\pi\pi^*$  state lies at 262 nm, i.e., close to 275 nm, and decays (10–20 fs) into the  $n\pi^*$ state, 46 which absorbs in the 345-370 nm region 47 and survives for  $\sim$ 2 ps before relaxing to  $S_0$ .

Induced absorption and bleach signals due to the formation of the *cis*-isomer of 4,4'-APy persist with no change up to 1 ns

following both 290 and 275 nm excitation (insets in Figure 3c,f). The relative quantum yields of the cis-isomer formation can be compared. At  $\sim$ 1 ps, the initially excited population is redistributed between  $TM_1 n\pi^*$  and hot  $S_0$  species. The ratio of the 410 nm  $\Delta A$  signal in the trans-cis difference spectrum to the 1 ps 390 nm  $\Delta A$  signal is  $3 \times 10^{-3}$ ,  $2.7 \times 10^{-2}$ , and  $5 \times 10^{-3}$  $10^{-2}$  for 460, 290, and 275 nm, respectively (Figure 26SI), indicating that 460 nm excitation disfavors the formation of cisisomers in comparison to the  $TM_1$   $n\pi^*$  species by a factor of 10. Because the hot S<sub>0</sub> signals in the case of 290 (275) nm excitation are larger only by a factor of 2-3 (cf. the  $\Delta A$ amplitudes in the 6 ps spectra upon 290 (275) nm and 460 nm excitation; Figures 2 and 3), one can conclude that *cis*-isomers become more favored upon going from visible to UV excitation. High repetition rate 460 and 290 nm irradiation experiments (Figure 4SI) give a similar trend.

The topography of the  $S_1$  and  $S_2$  PESs predicted for 3-PAPy<sup>32</sup> and the  $S_1$  PES predicted for 4-PAPy<sup>34</sup> may serve as a guide for 4,4'-APy (Figure 1b). For 3-PAPy,<sup>32</sup> the nonrotational path starting from the  $S_1$   $n\pi^*$  FC geometry is barrierless, leading to a local planar S<sub>1</sub> minimum separated by a small barrier from a very shallow minimum not far from a planar  $n\pi^*/S_0$  CI, where the local topology favors a return to the trans structure. A steeper path from the  $S_1 n\pi^*$  FC geometry leads to the rotated  $n\pi^*$  global minimum,  $^{32,34}$  where the dipoleforbidden  $n\pi^*$  and the dipole-allowed  $\pi\pi^*$  states strongly mix, and afterward continues to the rotated  $n\pi^*/S_0$  CI, where either trans- or cis-configurations can form. It is well-known that radiative  $S_1 \ n\pi^* \to S_0$  transitions become allowed when the  $n\pi^*$  state is vibrationally coupled to a dipole-allowed excited state. A pure CNNC torsion, the mode along which the photoisomerization is proposed to occur in azobenzene derivatives, is the most effective in inducing intensity in the  $S_1 n\pi^* \rightarrow S_0$  transition.<sup>14</sup> Consequently, the  $S_1 n\pi^* \rightarrow S_0$ radiative transition in the 3-PAPy global rotated minimum is predicted to have large oscillator strength.<sup>32</sup> Stimulated emission from this minimum should be detectable at  $\lambda \geq$ ~495 nm, which is within the probe range studied, but it is not observed. Further, the 300 fs lifetime is characteristic of a decay via avoided crossing, such as the TM2 region in the nonrotational path, and the fact that it is single-exponential is difficult to reconcile with barrierless relaxation. 48 This time scale is well beyond the typical sub-100 fs time scale of passage through a CI. 49 Therefore, we conclude that the relaxation pathway following  $n\pi^*$  excitation is nonrotational and assign the 2.1 ps lifetime to the local planar  $n\pi^*$  minimum, TM<sub>1</sub>. The remaining population evolves with 35-65 fs components describing position-dependent ESA and a single 300 fs time constant that describes its time-independent loss into S<sub>0</sub> through a shallow TM<sub>2</sub> minimum located further down the reaction coordinate at a small  $n\pi^*/S_0$  energy gap, where the local topology favors the return to the trans structure (Figure 1c).

The lifetime of the  $\pi\pi^*$  state in 4,4'-APy (~30 fs) determined in this work agrees with steep slopes of the FC  $\pi\pi^*$  region found in 3-PAPy.<sup>32</sup> The 30 fs lifetime appears much shorter compared to a vibrational period of reactive CNNC torsional motion<sup>14,20</sup> (a 54 cm<sup>-1</sup> frequency,<sup>14</sup> TAB S<sub>2</sub>  $\pi\pi^*$ ), which corresponds to a ~600 fs vibrational period. Therefore, the rotational pathway is unlikely to contribute into the  $\pi\pi^*$  decay in 4,4'-APy. The sub-100 fs observation of hot S<sub>0</sub> population is consistent with high-frequency vibrational modes populating the nonrotational path.

The dynamics of the 4,4'-APy system bears many similarities with that of TAB. For example, in TAB and azobenzene systems generally, <sup>7,12,13,50</sup> vibrational relaxation and cooling in the bottom of trans-S<sub>0</sub> give rise to a transient absorption feature below 400 nm that decays on a ~10 ps time scale. Our results do not provide any evidence that triplet states are involved in the reaction mechanism, as is the case for the photoisomerization of TAB. 6,29 We were able to resolve the lifetime of the  $\pi\pi^*$  state for 4,4'-APy in ethanol (30 fs), the decay of which is comparable with that for TAB in ethanol (lifetime,  $\sim 50 \text{ fs}^{17}$ ); the  $\pi\pi^*$  state decay correlates to the buildup of hot  $n\pi^*$  population in both systems. Several ultrafast transient absorption studies 10-13 reported that the  $n\pi^*$  decays in a biphasic fashion, e.g., with 0.34 and 3.0 ps time constants in ethanol. 12 The decay-associated spectra of these components were similar, and therefore, they were interpreted as arising from the same electronic state and assigned to a movement of the wavepacket generated by the optical excitation out of the FC region (recently identified as relaxation of the hot  $S_1$  state<sup>50</sup>) and the  $n\pi^*$  excited-state lifetime, respectively. When excited into the  $S_1$   $n\pi^*$  state, 4,4'-APy exhibits similar time constants (0.3 and 2.1 ps). The data suggest that they originate from the same  $n\pi^*$  state, but different regions, respectively, the exit channel (TM<sub>2</sub>) and the planar minimum (TM<sub>1</sub>) that determines the  $n\pi^*$  state lifetime.

An increase of the photoisomerization quantum yield upon  $\pi\pi^*$  excitation in 4,4'-APy is opposite to the trend in TAB where the photoisomerization quantum yield becomes halved. Several important points were brought up when rationalizing the trend observed for TAB, such as the quantum yield of  $\pi\pi^*$  $\rightarrow n\pi^*$  internal conversion should be equal to unity and the crossing point between these states has to be planar, 16 which, according to our analysis herein, are valid for 4,4'-APy as well. The recent study of TAB<sup>17</sup> proposed that following  $\pi\pi^* \rightarrow$  $n\pi^*$  internal conversion the hot  $n\pi^*$  population decays to the trans-S<sub>0</sub> state via a near-planar region of the  $n\pi^*/S_0$  CI seam inaccessible upon selective excitation of the  $n\pi^*$  state. Regarding 4,4'-APy, if the  $\pi\pi^*$  population were to decay only via the  $TM_1$  and  $TM_2$ , like in the  $n\pi^*$  case, similar photoisomerization quantum yields would be expected upon  $n\pi^*$  and  $\pi\pi^*$  excitations, which contrasts with a larger yield observed upon  $\pi\pi^*$  excitation. An explanation is that in 4,4'-APy the high-energy planar  $n\pi^*/S_0$  crossing, which is not accessible from the  $n\pi^*$  FC region, favors the cis-S<sub>0</sub> state more readily than the region of the same crossing accessible upon  $n\pi^*$  excitations (Figure 4f). Irrespective of the involvement of the pyridine-localized states at 275 nm (Figure 27SI), a larger photoisomerization quantum yield upon 275 nm in comparison to 290 nm excitation supports the above suggestion, further suggesting that the effect increases with excitation energy. For TAB, coherent dynamics due to 195 cm<sup>-1</sup> vibrational coherence in the CNN in-plane bending mode was observed in the  $n\pi^*$  state after  $\pi\pi^* \rightarrow n\pi^*$  internal conversion. For 4,4'-APy, very similar vibrational coherence in the product  $n\pi^*$  state is observed, providing evidence for the nonrotational  $\pi\pi^* \rightarrow n\pi^*$  internal conversion pathway. Whereas the CNN in-plane bending channel is nonreactive and the prime reason for the quantum yield reduction at shorter excitation wavelengths in TAB, 17 for 4,4'-APy this active channel is reactive. In 4,4'-APy, the same vibrational coherence (frequency, 195 cm<sup>-1</sup>) is also observed upon selective  $n\pi^*$  excitation, consistent with a common excitedstate pathway that the system takes upon  $\pi\pi^*$  and  $n\pi^*$ 

excitation. Our results suggest that 195 cm<sup>-1</sup> coherent dynamics can serve as a fingerprint of the CNN in-plane bending relaxation channel in excited states of  $\pi\pi^*$  and  $n\pi^*$  nature in azobenzene derivatives.

#### ASSOCIATED CONTENT

#### **Solution** Supporting Information

The Supporting Information is available free of charge at https://pubs.acs.org/doi/10.1021/acs.jpclett.2c02523.

UV—vis absorption spectrum of 4,4'-APy, continuous irradiation measurements, description of ultrafast transient absorption experiments, data at different excitation wavelengths, FFT analysis of vibrational coherences, time constants from multiexponential fitting of transient absorption kinetic traces, decoherence time constants, and comparison of different relaxation mechanisms for 4,4'-APy (PDF)

#### AUTHOR INFORMATION

#### **Corresponding Authors**

Patrick Z. El-Khoury — Physical Sciences Division, Pacific Northwest National Laboratory, Richland, Washington 99354, United States; orcid.org/0000-0002-6032-9006; Email: Patrick.ElKhoury@pnnl.gov

Alexander N. Tarnovsky — Department of Chemistry and the Center for Photochemical Sciences, Bowling Green State University, Bowling Green, Ohio 43403, United States; Orcid.org/0000-0001-7918-2676; Email: atarnov@bgsu.edu

#### Author

Laura M. Obloy — Department of Chemistry and the Center for Photochemical Sciences, Bowling Green State University, Bowling Green, Ohio 43403, United States; ocid.org/0000-0001-8935-948X

Complete contact information is available at: https://pubs.acs.org/10.1021/acs.jpclett.2c02523

#### Notes

The authors declare no competing financial interest.

#### ACKNOWLEDGMENTS

This work was supported by the NSF (CHE-2102619, CHE-0923360, and CHE-1626420) and BGSU "Building Strength" grants. Dr. Patrick Z. El-Khoury acknowledges support from the Laboratory Directed Research and Development Program at Pacific Northwest National Laboratory. We thank Dr. Darya S. Budkina (BGSU) for assistance with UV pulse compression and Dr. Kevin T. Crampton (PNNL) for several useful discussions.

#### REFERENCES

- (1) Bandara, H. M. D.; Burdette, S. C. Photoisomerization in Different Classes of Azobenzene. *Chem. Soc. Rev.* **2012**, *41*, 1809–1825.
- (2) Kamiya, Y.; Asanuma, H. Light-Driven DNA Nanomachine with a Photoresponsive Molecular Engine. *Acc. Chem. Res.* **2014**, *47*, 1663–1672
- (3) Mahimwalla, Z.; Yager, K. G.; Mamiya, J.; Shishido, A.; Priimagi, A.; Barrett, C. J. Azobenzene Photomechanics: Prospects and Potential Applications. *Polym. Bull.* **2012**, *69*, 967–1006.

- (4) Garcia-Amorós, J.; Maerz, B.; Reig, M.; Cuadrado, A.; Blancafort, L.; Samoylova, E.; Velasco, D. Picosecond Switchable Azo Dyes. *Chem.—Eur. J.* **2019**, *25*, 7726–7732.
- (5) Das, D.; Yadav, M. K.; Singla, L.; Kumar, A.; Karanam, M.; Dev, S.; Choudhury, A. R. Understanding of the Kinetic Stability of *cis*-Isomer of Azobenzenes through Kinetic and Computational Studies. *ChemistrySelect* **2020**, *5*, 13957–13962.
- (6) Casellas, J.; Bearpark, M. J.; Reguero, M. Excited-State Decay in the Photoisomerisation of Azobenzene: A New Balance between Mechanisms. *ChemPhysChem.* **2016**, *17*, 3068–3079.
- (7) Fujino, T.; Tahara, T. Picosecond Time-Resolved Raman Study of trans-Azobenzene. J. Phys. Chem. A 2000, 104, 4203-4210.
- (8) Fujino, T.; Arzhantsev, S. Y.; Tahara, T. Femtosecond Time-Resolved Fluorescence Study of Photoisomerization of *trans*-Azobenzene. *J. Phys. Chem. A* **2001**, *105*, 8123–8129.
- (9) Chang, C.-W.; Lu, Y.-C.; Wang, T.-T.; Diau, E.-G. Photoisomerization Dynamics of Azobenzene in Solution with  $S_1$  Excitation: A Femtosecond Fluorescence Anisotropy Study. *J. Am. Chem. Soc.* **2004**, 126, 10109–10118.
- (10) Nägele, T.; Hoche, R.; Zinth, W.; Wachtveitl, J. Femtosecond Photoisomerization of *cis*-Azobenzene. *Chem. Phys. Lett.* **1997**, 272, 489–495
- (11) Lednev, I. K.; Ye, T.-Q.; Matousek, P.; Towrie, M.; Foggi, P.; Neuwahl, F. V. R.; Umapathy, S.; Hester, R. E.; Moore, J. N. Femtosecond Time-Resolved UV-Visible Absorption Spectroscopy of trans-Azobenzene: Dependence on Excitation Wavelength. *Chem. Phys. Lett.* **1998**, 290, 68–74.
- (12) Satzger, H.; Spörlein, S.; Root, C.; Wachtveitl, J.; Zinth, W.; Gilch, P. Fluorescence Spectra of *trans* and *cis*-Azobenzene Emission from the Franck–Condon State. *Chem. Phys. Lett.* **2003**, 372, 216–223.
- (13) Quick, M.; Dobryakov, A. L.; Gerecke, M.; Richter, C.; Berndt, F.; Ioffe, I. N.; Granovsky, A. A.; Mahrwald, R.; Ernsting, N. P.; Kovalenko, S. A. Photoisomerization Dynamics and Pathways of *trans* and *cis* Azobenzene in Solution from Broadband Femtosecond Spectroscopies and Calculations. *J. Phys. Chem. B* **2014**, *118*, 8756–8771.
- (14) Tan, E. M. M.; Amirjalayer, S.; Smolarek, S.; Vdovin, A.; Zerbetto, F.; Buma, W. J. Fast Photodynamics of Azobenzene Probed by Scanning Excited-State Potential Energy Surfaces using Slow Spectroscopy. *Nat. Commun.* **2015**, *6*, 5860–5865.
- (15) Chowdary, P. D.; Umapathy, S. Ultrafast Dynamics and Photochemistry of  $\pi \pi^*$  Excited *trans*-Azobenzene A Comprehensive Analysis of Resonance Raman Intensities. *J. Raman Spectrosc.* **2008**, *39*, 1538–1555.
- (16) Schultz, T.; Quenneville, J.; Levine, B.; Toniolo, A.; Martínez, T. J.; Lochbrunner, S.; Schmitt, M.; Shaffer, J. P.; Zgierski, M. Z.; Stolow, A. Mechanism and Dynamics of Azobenzene Photoisomerization. *J. Am. Chem. Soc.* **2003**, *125*, 8098–8099.
- (17) Nenov, A.; Borrego-Varillas, R.; Oriana, A.; Ganzer, L.; Segatta, F.; Conti, I.; Segarra-Marti, J.; Omachi, J.; Dapor, M.; Taioli, S.; Manzoni, C.; Mukamel, S.; Cerullo, G.; Garavelli, M. UV-Light-Induced Vibrational Coherences: The Key to Understand Kasha Rule Violation in *trans*-Azobenzene. *J. Phys. Chem. Lett.* **2018**, *9*, 1534–1541.
- (18) Diau, E. W.-D. A New Trans-to-Cis Photoisomerization Mechanism of Azobenzene on the  $S_1(n,\pi^*)$  Surface. *J. Phys. Chem. A* **2004**, *108*, 950–956.
- (19) Conti, I.; Garavelli, M.; Orlandi, G. The Different Photoisomerization Efficiency of Azobenzene in the Lowest  $n\pi^*$  and  $\pi\pi^*$  Singlets: The Role of a Phantom State. *J. Am. Chem. Soc.* **2008**, *130*, 5216–5230.
- (20) Gámez, J. A.; Weingart, O.; Koslowski, A.; Thiel, W. Cooperating Dinitrogen and Phenyl Rotations in *trans*-Azobenzene Photoisomerization. *J. Chem. Theory Comput.* **2012**, *8*, 2352–2358.
- (21) Xu, C.; Yu, L.; Gu, F. L.; Zhu, C. Probing the  $\pi \to \pi^*$  Photoisomerization Mechanism of *trans*-Azobenzene by Multi-State *ab initio* on-the-Fly Trajectory Dynamics Simulations. *Phys. Chem. Phys.* **2018**, 20, 23885–23897.

- (22) Pederzoli, M.; Pittner, J.; Barbatti, M.; Lischka, H. Nonadiabatic Molecular Dynamics Study of the *cis-trans* Photoisomerization of Azobenzene Excited to the S<sub>1</sub> State. *J. Phys. Chem.* A **2011**, 115, 11136–11143.
- (23) Yu, L.; Xu, C.; Lei, Y.; Zhu, C.; Wen, Z. Trajectory-Based Nonadiabatic Molecular Dynamics without Calculating Nonadiabatic Coupling in the Avoided Crossing Case: trans ↔ cis Photoisomerization in Azobenzene. *Phys. Chem. Chem. Phys.* **2014**, *16*, 25883−25895.
- (24) Yu, J. K.; Bannwarth, C.; Liang, R.; Hohenstein, E. G.; Martínez. Nonadiabatic Dynamics Simulation of the Wavelength-Dependent Photochemistry of Azobenzene Excited to the  $n\pi^*$  and  $\pi\pi^*$  Excited States. *J. Am. Chem. Soc.* **2020**, *142*, 20680–20690.
- (25) Yuan, S.; Dou, Y.; Wu, W.; Hu, Y.; Zhao, J. Why Does trans-Azobenzene Have a Smaller Isomerization Yield for  $\pi\pi^*$  Excitation than for  $n\pi^*$  Excitation? *J. Phys. Chem. A* **2008**, *112*, 13326–13334.
- (26) Cattaneo, P.; Persico, M. An *ab initio* Study of the Photochemistry of Azobenzene. *Phys. Chem. Chem. Phys.* **1999**, *1*, 4739–4743.
- (27) Cembran, A.; Bernardi, F.; Garavelli, M.; Gagliardi, L.; Orlandi, G. On the Mechanism of the cis trans Isomerization in the Lowest Electronic States of Azobenzene: S<sub>0</sub>, S<sub>1</sub>, and T<sub>1</sub>. *J. Am. Chem. Soc.* **2004**, *126*, 3234–3243.
- (28) Ishikawa, T.; Noro, T.; Shoda, T. Theoretical Study on the Photoisomerization of Azobenzene. *J. Chem. Phys.* **2001**, *115*, 7503–7512.
- (29) Griffiths, J., II. Photochemistry of Azobenzene and its Derivatives. *Chem. Soc. Rev.* **1972**, *1*, 481–493.
- (30) Rau, H.; Lüddecke, E. On the Rotation Inversion Controversy on Photoisomerization of Azobenzenes. Experimental Proof of Inversion. *J. Am. Chem. Soc.* **1982**, *104*, 1616–1620.
- (31) Venkataramani, S.; Jana, U.; Dommaschk, M.; Sönnichsen, F.; Tuczek, F.; Herges, R. Magnetic Bistability of Molecules in Homogeneous Solution at Room Temperature. *Science* **2011**, *331*, 445–448.
- (32) Casellas, J.; Alcover-Fortuny, G.; de Graaf, C.; Reguero, M. Phenylazopyridine as Switch in Photochemical Reactions. A Detailed Computational Description of the Mechanism of Its Photoisomerization. *Materials* **2017**, *10*, 1342–1357.
- (33) Alcover-Fortuny, G.; de Graaf, C.; Caballol, R. Spin-Crossover in Phenylazopyridine-Functionalized Ni–Porphyrin: trans-cis Isomerization Triggered by  $\pi-\pi$  Interactions. *Phys. Chem. Chem. Phys.* **2015**, *17*, 217–225.
- (34) Wang, L.; Yi, C.; Zou, H.; Xu, J.; Xu, W. Theoretical Study on the Isomerization Mechanisms of Phenylazopyridine on S<sub>0</sub> and S<sub>1</sub> States. *J. Phys. Org. Chem.* **2009**, 22, 888–896.
- (35) Bannwarth, A.; Schmidt, S. O.; Peters, G.; Sönnichsen, F. D.; Thimm, W.; Herges, R.; Tuczek, F. Fe<sup>III</sup> Spin-Crossover Complexes with Photoisomerizable Ligands: Experimental and Theoretical Studies on the Ligand-Driven Light-Induced Spin Change Effect. *Eur. J. Inorg. Chem.* **2012**, 2012, 2776–2783.
- (36) Zewail, A. H. Femtochemistry. J. Phys. Chem. 1993, 97, 12427—12446.
- (37) Vöhringer, P.; Westervelt, R. A.; Yang, T.-S.; Arnett, D. C.; Feldstein, M. J.; Scherer, N. F. Solvent and Frequency Dependence of Vibrational Dephasing on Femtosecond Time-Scales. *J. Raman Spectrosc.* **1995**, 26, 535–551.
- (38) Pollard, W. T.; Mathies, R. A. Analysis of Femtosecond Dynamic Absorption Spectra of Nonstationary States. *Annu. Rev. Phys. Chem.* **1992**, 43, 497–523.
- (39) Wang, Q.; Schoenlein, R. W.; Peteanu, L. A.; Mathies, R. A.; Shank, C. V. Vibrationally Coherent Photochemistry in the Femtosecond Primary Event of Vision. *Science* 1994, 266, 422–424.
- (40) Vos, M. H.; Jones, M. R.; Martin, J.-L. Vibrational Coherence in Bacterial Reaction Centers: Spectroscopic Characterization of Motions Active during Primary Electron Transfer. *Chem. Phys.* **1998**, 233, 179–190.

- (41) Liebl, U.; Lipowski, G.; Négrerie, M.; Lambry, J.-C.; Martin, J.-L.; Vos, M. H. Coherent Reaction Dynamics in a Bacterial Cytochrome C Oxidase. *Nature* **1999**, *401*, 181–184.
- (42) Elsaesser, A.; Kaiser, W. Vibrational and Vibronic Relaxation of Large Polyatomic Molecules in Liquids. *Annu. Rev. Phys. Chem.* **1991**, 42, 83–107.
- (43) Kliner, D. A. V.; Alfano, J. C.; Barbara, P. F. Photodissociation and Vibrational Relaxation of I<sub>2</sub><sup>-</sup> in Ethanol. *J. Chem. Phys.* **1993**, *98*, 5375–5389.
- (44) Fuß, W. Where Does the Energy Go in fs-Relaxation? *Chem. Phys.* **2013**, 425, 96–103.
- (45) Bultmann, T.; Ernsting, N. P. Competition between Geminate Recombination and Solvation of Polar Radicals following Ultrafast Photodissociation of Bis(*p*-aminophenyl) Disulfide. *J. Phys. Chem.* **1996**, *100*, 19417–19424.
- (46) Yang, J.; Zhu, X.; Nunes, J. P. F.; Yu, J. K.; Parrish, R. M.; Wolf, T. J. A.; Centurion, M.; Gühr, M.; Li, R.; Liu, Y.; Moore, B.; Niebuhr, M.; Park, S.; Shen, X.; Weathersby, S.; Weinacht, T.; Martinez, T. J.; Wang, X. Simultaneous Observation of Nuclear and Electronic Dynamics by Ultrafast Electron Diffraction. *Science* **2020**, 368, 885–889.
- (47) Chachisvilis, M.; Zewail, A. H. Femtosecond Dynamics of Pyridine in the Condensed Phase: Valence Isomerization by Conical Intersections. *J. Phys. Chem. A* **1999**, *103*, 7408–7418.
- (48) Bagchi, B.; Fleming, G. R. Dynamics of Activationless Reactions in Solution. *J. Phys. Chem.* **1990**, *94*, 9–20.
- (49) Polli, D.; Altoè, P.; Weingart, O.; Spillane, K. M.; Manzoni, C.; Brida, D.; Tomasello, G.; Orlandi, G.; Kukura, P.; Mathies, R. A.; Garavelli, M.; Cerullo, G. Conical Intersection Dynamics of the Primary Photoisomerization Event in Vision. *Nature* **2010**, *467*, 440–442
- (50) Otolski, C. J.; Raj, A. M.; Ramamurthy, V.; Elles, C. G. Ultrafast Dynamics of Encapsulated Molecules Reveals New Insight on the Photoisomerization Mechanism for Azobenzenes. *J. Phys. Chem. Lett.* **2019**, *10*, 121–127.

### ☐ Recommended by ACS

## Computational Exploration of the Intersystem Crossing from the $X^3A_2$ to the $\tilde{a}^1A_1$ State in Boryl Nitrenes upon Photoexcitation

Virinder Bhagat and Holger F. Bettinger

OCTOBER 18, 2022

THE JOURNAL OF PHYSICAL CHEMISTRY A

RFAD 🗹

### Reversible, Red-Shifted Photoisomerization in Protonated Azobenzenes

Jonas Rickhoff, Luuk Kortekaas, et al.

AUGUST 03, 2022

THE JOURNAL OF ORGANIC CHEMISTRY

READ 🗹

#### Photon Energy Storage in Strained Cyclic Hydrazones: Emerging Molecular Solar Thermal Energy Storage Compounds

Qianfeng Qiu, Grace G. D. Han, et al.

JULY 08, 2022

JOURNAL OF THE AMERICAN CHEMICAL SOCIETY

READ 🗹

## Inclusion-Activated Reversible *E/Z* Isomerization of a Cyanostilbene Derivative Based on Cucurbit[8]uril under 365 nm Ultraviolet Irradiation

Xiaohan Sun, Yu Liu, et al.

JUNE 06, 2022

THE JOURNAL OF ORGANIC CHEMISTRY

READ 🗹

Get More Suggestions >